Chemico-Biological Interactions xxx (2015) xxx–xxx

Contents lists available at ScienceDirect

Chemico-Biological Interactions

journal homepage: www.elsevier.com/locate/chembioint

Oxalic acid capped iron oxide nanorods as a sensing platform

Anshu Sharma [a,b], Dinesh Baral [b], H.B. Bohidar [a,b,*], Pratima R. Solanki [a,*]

[a] Special Centre for Nanosciences, Jawaharlal Nehru University, New Delhi 110067, India
[b] School of Physical Science, Jawaharlal Nehru University, New Delhi 110067, India

ARTICLE INFO

Article history:
Received 9 March 2015
Received in revised form 12 May 2015
Accepted 29 May 2015
Available online xxxx

Keywords:
Oxalic acid
Monoclonal antibodies
Biosensor
Iron oxide nanoparticles
Electrochemical studies

ABSTRACT

A label free impedimetric immunosensor has been fabricated using protein bovine serum albumin (BSA) and monoclonal antibodies against *Vibrio cholerae* (Ab) functionalized oxalic acid (OA) capped iron oxide (Fe_3O_4) nanorods for *V. cholerae* detection. The structural and morphological studies of Fe_3O_4 and OA-Fe_3O_4/ITO, were characterized by X-ray diffraction (XRD), transmission electron microscopy (TEM), Fourier transform infrared (FTIR) spectroscopy and dynamic light scattering (DLS) techniques. The average crystalline size of Fe_3O_4, OA-Fe_3O_4 nanorods were obtained as about 29 ± 1 and 39 ± 1 nm, respectively. The hydrodynamic radius of nanorods is found as 116 nm (OA-Fe_3O_4) and 77 nm (Fe_3O_4) by DLS measurement. Cytotoxicity of Fe_3O_4 and OA-Fe_3O_4/ITO nanorods has been investigated in the presence of human epithelial kidney (HEK) cell line 293 using MTT assay. The cell viability and proliferation studies reveal that the OA-Fe_3O_4 nanorods facilitate cell growth. The results of electrochemical response studies of the fabricated BSA/Ab/OA-Fe_2O_3/ITO immunosensor exhibits good linearity in the range of 12.5–500 ng mL^{-1} with low detection limit of 0.5 ng mL^{-1}, sensitivity 0.1 Ω/ng ml^{-1} cm^{-2} and reproducibility more than 11 times.

1. Introduction

Recently, investigators are being utilizing several types of nanostructured materials including iron oxides (mostly maghemite, γ-Fe_2O_3 and α-Fe_2O_3 or magnetite, Fe_3O_4), among which magnetite is a very promising candidate. These iron oxide nanomaterials exhibits wide applications in various fields including electronic devices, drug delivery, ferrofluid technology, contrast agents hyperthermia treatment, cell separation, enzymatic assays biosensors, etc. [1–9] due to their peculiar physical and electronics properties such as small size, super-magnetic, low toxicity, biocompatibility and stability under physiological conditions. Although, these materials are more susceptibility towards oxidation and their tendency to agglomerate due to availability of strong dipole–dipole interactions between particles which can be prevented by functionalization with other materials [10]. The proper functionalization of nanomaterial with desire solvent is important to prevent aggregation and obtain thermodynamically stable nanoparticles. Thus, this nanomaterial can be functionalized with different materials including chitosan, carbon, polymers, surfactants, bio-molecules, silica, metals, small polar molecules including citric acid (CA) etc. [2,11,12] which provide improved stability and biocompatibility nanoparticles. Moreover, the functionalized nanoparticles with carbon and silica capped α Fe_3O_4 and γ-Fe_2O_3 NPs control the phase transition of Fe_3O_4 nanorods at the time of electrophoretic film deposition and provide improved the electrochemical properties [2].

It has been observed that nanomaterial functionalized with carboxylic acid terminal group exhibit great importance because carboxyl group not only render the particles more water dispersible but also provides a site for further surface modification that can be utilized for wide applications including biomedical [13–17]. In this context, carboxylic group containing small molecules like oxalic acid (OA; $C_2H_2O_2$, OA) and citric acid (CA; $C_6H_8O_7$) found more suitable for functionalization of Fe_3O_4 nanorods. Because, OA and CA can be adsorbed onto the surface of the nanomaterial by coordinating *via* one or two of the carboxylate functionalities, leaving at least one carboxylic acid group exposed, making the nanomaterial surface hydrophilic, preventing particle agglomeration, and providing other functional groups to be used for further surface modification including oligonucleotides and antibodies or proteins *via* covalent bonding [18]. It has been observed that most of studies reported in literature are based on CA coated iron oxide nanomaterial for their biomedical applications including in contrast agent, drug delivery, targeted cellular imaging, hyperthermia and

* Corresponding authors at: Special Centre for Nanosciences, Jawaharlal Nehru University, New Delhi 110067, India (H.B. Bohidar). Tel.: +91 11 26704740, +91 11 26704699.
E-mail addresses: bohidarjnu@gmail.com (H.B. Bohidar), partima@mail.jnu.ac.in (P.R. Solanki).

http://dx.doi.org/10.1016/j.cbi.2015.05.020
0009-2797/

biodetection [10,11,19]. De Sousa has been reported that CA coated nanoparticles (NPs) stable in water and suitable for energy dissipation under an external ac magnetic field in the *rf* range which appropriated for magnetic hyperthermia therapy [20]. Cheraghipour et al., reported that CA capped NPs exhibit remarkable heating effect during the application of a magnetic field, which make them attractive for magnetic fluid hyperthermia applications [21]. NPs coated with both oleic acid and pluronic loaded with high doses of hydrophobic drugs has been used for drug delivery [22]. Oxalic acid (OA), has gained importance in green chemistry organic oxalic acid is essential for human body. The OA has been utilized as a reductant for silver nanoparticles synthesis and stabilizing by cetyltrimethyl-ammonium bromide (CTAB). Thus there is a wide scope to explore the studies on OA functionalized Fe_3O_4 for electrochemical biosensing applications.

Here, we have fabricated *in situ* capped OA-Fe_3O_4 nanorods for immunosensor application. A thin film of OA-Fe_3O_4 nanorods has been prepared using electrophoretic deposition technique onto Indium-tin-oxide (ITO) coated glass substrate and utilized for functionalization with monoclonal antibodies specific towards the *Vibrio cholerae* and bovine serum albumin (BSA) for *V. cholerae* detection using impedimetric spectroscopic technique. *V. cholerae* is known to be highly pathogenic which creates a serious health problem like diarrhea and acidosis in human. Thus, development of point of care devices has recently gained increasing attention in diverse fields including clinical diagnosis, environmental monitoring and food safety etc. [23,24]. Few immunosensors have been reported based on nanostructured materials for *V. cholerae* detection [25–28]. To the best of our knowledge, this is first time report on OA capped synthesized Fe_3O_4 nanorods and even for fabrication of immunosensor for pathogen (*V. cholerae*) detection. These 1D nanomaterials (OA-Fe_3O_4) nanorods provide direct attachment of antibodies *via* electrostatic interactions that may preserve the structural integrity of the antibodies resulted in higher sensitivity as compared to CA capped Fe_3O_4 nanoparticles [19]. Moreover, the cytotoxicity effect of Fe_3O_4 nanorods is still unexplored for application to point-of-care devices.

2. Experimental section

2.1. Material and methods

$FeCl_3$ (Fe^{3+}); $FeCl_2$ (Fe^{2+}) and NaOH was purchased from Fisher Scientific Ltd. Oxalic acid (OA; $C_2H_2O_4$) was purchased from SDFCL, Mumbai-30. All these chemicals were used to prepare solutions in deionized water without further purification. Indium-tin-oxide (ITO) coated glass plates were obtained from Balzers, UK, (Baltracom 247 ITO, 1.1 mm thick) with a sheet resistance and transmittance of 25 $\Omega\,sq^{-1}$ and 90%, respectively. Monoclonal antibodies specific to *V. cholerae* (Ab-Vc) and bovine serum albumin (BSA) have been obtained from M/s Genetix Biotech Asia Pvt. Ltd, India. All other chemicals were of analytical grade and used without further purification. Deionized water from Organo Biotech Laboratories, India, was used to prepare the solutions.

2.2. Preparation of OA capped Iron oxide nanorods

The magnetite nanorods have been prepared using co-precipitation technique which is the simpler process followed by as reported in literatures [29]. We have used 0.2 M (25 mL) of $FeCl_3$ and 0.1 M (25 mL) of $FeCl_2$ and dissolved in de-ionized water with stirring, the proposed reaction is give below (1). The capping was done by maintaining the 1:1 ratio of resulting solution and the capping agent (OA) of 0.5 gm (10 mL^{-1}) was added drop wise followed by continuous stirring at 80 °C. Then NaOH solution of 2 M (100 mL) was added drop wise at 90 °C with vigorously stirring for 30 min as reported by [30]. The precipitating agent is NaOH solution (basic medium). Thus obtained dark brown precipitation is taken for magnetic decantation and washed several times with de-ionized water until the pH 7 was noted. Here bare magnetite nanorods were prepared without the functionalization, means the capping agent (oxalic acid; OA) are not dissolved in the salt solution. The same procedure is followed to obtain the bare magnetite particle.

The principle reaction for the co-precipitation method is:

$$Fe^{2+} + 2Fe^{3+} + 8\,OH^- \rightarrow Fe_3O_4 + 4\,H_2O \quad (1)$$

2.3. Cell proliferation study

The biocompatibility test of bare Fe_3O_4 and OA-Fe_3O_4 has been monitored on cells line survival/proliferation (human epithelial kidney cell line HEK 293) was studied using Methyl Thiazol Tetrazolium (MTT) assay. HEK 293 is used as test cell line. The HEK 293 cells are procured from NCC, Pune, India. The cells are maintained in completed growth medium [10% FBS containing Dulbecco's Modified Eagle's Medium (DMEM) medium] at 37 °C under humidified 5% CO_2 environment. For the assay, cells were plated at about 6000/well in 96-well tissue-culture plate and were allowed to attach for 48 h. Next day, the medium on cells was replaced with MTT containing DMEM medium. The cells were kept for 6 h at 37 °C to allow reduction of MTT dye to formazan crystals by living cells. Cells in each wells were solubilized in 200 μL of dimethyl sulfoxide (DMSO), followed by absorbance measurement at 570 nm. The% change in proliferation was calculated with respect to control cells that were not exposed to NPs (control). All experiments were done in triplicates.

2.4. Preparation of OA-Fe_3O_4/ITO electrodes by electrophoretic deposition (EPD)

The thin film of OA-Fe_3O_4/ITO was deposited on onto the ITO surface using electrophoretic deposition (EPD) technique using a DC battery (BioRad, model 200/2.0) as the power supply. 0.25 mg of OA caped Fe_3O_4 (OA-NPs) was dispersed in 10 mL acetonitrile solution and ultra-sonicated for 30 min. To increase the deposition rate of nanorods onto the ITO surface Mg ions enhance the positive charge on the material surface which help in transportation of OA-Fe_3O_4 towards the cathode surface [26,31]. A platinum foil (1 cm × 2 cm) was used as an anode and a hydrolyzed ITO-coated glass plate as a cathode. The two electrodes, placed parallel to each other with a separation of 1 cm, were dipped in caped Fe_3O_4, NPs colloidal suspension. We have optimized the film deposition onto an ITO plate (0.25 cm^2) at different voltages ranging from 30 to 60 V for 40 s and then removed from the suspension followed by washing with de-ionized water to remove any unbound particles.

2.5. Biofunctionalization of OA-Fe_3O_4/ITO electrodes with antibodies (Ab) and BSA

The OA-Fe_3O_4/ITO electrodes were functionalized with monoclonal anti-*Vibrio cholera* antibodies (Ab). The stock solution of monoclonal antibodies specific towards *V. cholerae* (Ab; 1 ng mL^{-1}) was freshly prepared in phosphate buffer (50 mM, pH 7.0) and antigen (*V. cholerae*, Vc) aliquot in different working concentrations (1–500 ng mL^{-1}). 10 μL of Ab (1 ng mL^{-1}) solution was uniformly loaded onto OA-Fe_3O_4/ITO electrode surface *via* physical absorption and kept undisturbed overnight in a humid chamber.

Please cite this article in press as: A. Sharma et al., Oxalic acid capped iron oxide nanorods as a sensing platform, Chemico-Biological Interactions (2015), http://dx.doi.org/10.1016/j.cbi.2015.05.020

The positive charge OA-Fe_3O_4 NPs was electrostatically bound with the Fc region of antibodies (Ab). Then, these immunoelectrodes was immersed in 50 mM phosphate buffer saline (PBS) (pH 7.0, 0.9% KCl) to removed unbound antibodies from the surface. Finally, Ab/OA-Fe_3O_4/ITO immunoelectrode was treated with 10 μL (1 mg mL^{-1}) bovine serum albumin (BSA, 98%) solution for about 4 h to block the nonspecific site onto electrode surface. This BSA/Ab/OA-Fe_3O_4/ITO immunoelectrode was stored at 4 °C when not in use. Schematic 1 shows the step wise fabrication of OA-Fe_3O_4/ITO electrode and their modification with antibodies (Ab) and BSA for the detection of *Vc* concentration (see Scheme 1).

2.6. Characterizations

The structure, shape and crystallite size of synthesized Fe_3O_4 and OA-Fe_3O_4 nanorods were investigated by X-ray diffractometer (XRD, Rigaku D/Max 2200 diffractometer with CuKα radiation at $\lambda = 1.5406$ Å). Scanning electron microscope with dispersive X-ray spectroscopy (SEM, Zeiss, EVO, 40), high-resolution transmission electron microscope (HRTEM) images and selected area electron diffraction (SAED) studies were carried out using a JEOL JEM-2200 FS (Japan) instrument operating at a voltage of 200 kV. Samples for TEM analysis were prepared by spreading a drop of as-prepared products dilute dispersion on amorphous carbon-coated copper grids and then dried in air at room temperature. Fourier transform infrared spectroscopy (FT-IR) spectra of Ab/OA-Fe_3O_4/ITO immunoelectrodes were recorded on a Varian 7000 FT. Dynamic light scattering (DLS) measurements were performed at a scattering angle of $\theta = 90°$ and laser wavelength of He/Ne laser of $\lambda = 632.8$ nm on RINA Netzwerk RNA-technologies. The probe length scale is defined by the inverse of the modulus of the scattering wave vector q where the wave vector $q = (4\pi n/\lambda)\sin(\theta/2)$, the medium refractive index is n, the excitation wavelength is λ (=632.8 nm) and θ is the scattering angle. Further details on dynamic light scattering can be obtained from Berne and Pecora [32]. The instrument was used in the polarized mode to determine the particle size of particles. In all experiments, the difference between the measured and calculated baseline was not allowed to go beyond ±0.1%. The data that showed excessive baseline difference were rejected. Analysis of the measured correlation function yields the translational diffusion coefficient of the scattering moiety.

The diffusion coefficient is related to corresponding effective hydrodynamic radius through the Stoke–Einstein relation

$$R_h = \frac{k_B T}{6\pi\eta D} \quad (2)$$

where, the solvent viscosity is η, k_B is the Boltzmann constant, and T is the absolute temperature.

The zeta-potential measurements were performed on an electrophoresis instrument (model ZC-2000, Microtec, Japan). The solutions were diluted to know the surface charge of streaming particles. In the case of the interacting solutions, if one uses the zeta potential (Z) as an approximation of the surface potential φ of a uniformly charged sphere, the theory gives

$$Z \approx \varphi = 4\pi(\sigma/\varepsilon\kappa) \quad (3)$$

where σ is the surface charge density of the particle, and ε and κ are the dielectric constant and Debye–Huckel parameter of the solution, respectively. It has been shown to a very good approximation that the surface potential can be determined from the potential existing at the hydrodynamic slip plane, which is called the zeta potential. The relationship between the mobility (μ) and the zeta potential is $Z = 4\pi(\mu\eta/\varepsilon)$. Next, μ can be written as $\mu = \sigma/\eta\kappa$, where η is the viscosity of the solution [33,34].

Electrochemical studies [cyclic voltammetry (CV) and impedance] were conducted on an Autolab Potentiostat/Galvanostat (Eco Chemie, Netherlands) using a three-electrode cell using ITO as working electrode, platinum (Pt) foil as the auxiliary electrode and Ag/AgCl as reference electrode in phosphate buffer saline (PBS, pH7.0, 0.9% KCl) containing 3.3 mM $[Fe(CN)_6]^{3-/4-}$ as redox probe.

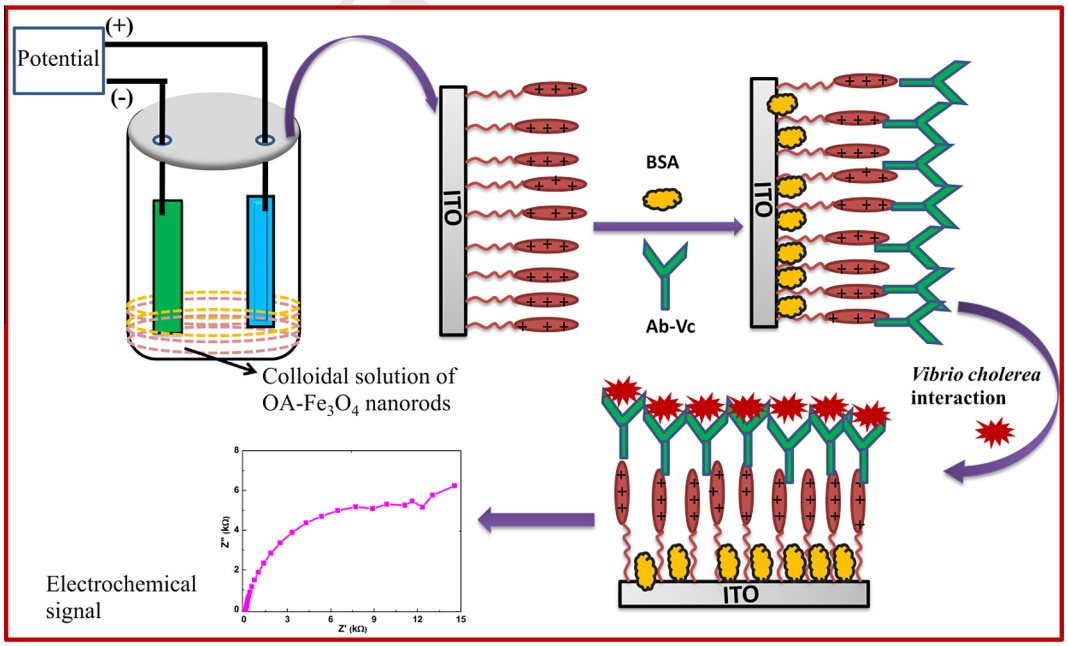

Scheme 1. The preparation of BSA/Ab/OA-Fe_3O_4/ITO immunoelectrode.

Please cite this article in press as: A. Sharma et al., Oxalic acid capped iron oxide nanorods as a sensing platform, Chemico-Biological Interactions (2015), http://dx.doi.org/10.1016/j.cbi.2015.05.020

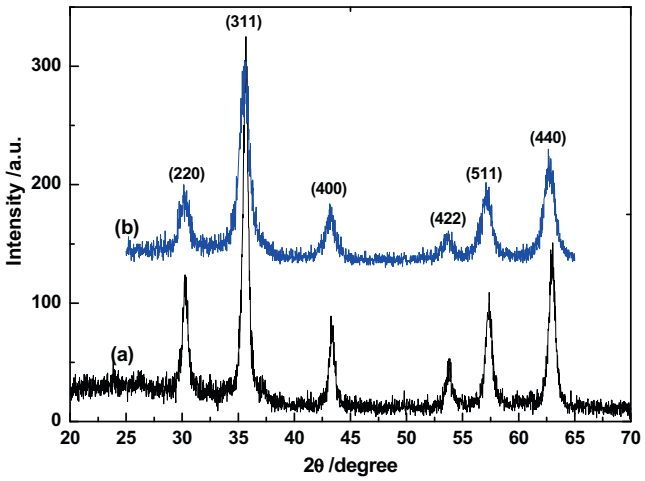

Fig. 1. X-ray diffraction pattern of (a) Fe_3O_4 and (b) OA-Fe_3O_4 nanorods.

3. Results and discussion

3.1. Characterization of OA-Fe_3O_4 nanocrystals

Fig. 1 shows the XRD studies of the Fe_3O_4, OA-Fe_3O_4 revealed the purity and crystallinity of the synthesized NPs with the cubic structure [space group: Fd-3 m] known for the Fe_3O_4 crystal (JCPDS Card No. 32-0483) [33,34]. It has been observed that the XRD pattern of bare and caped magnetite nanorods showed numbers of Braggs reflections that may be indexed on the basis of the face cantered cubic structure of NPs diffraction peaks corresponding to the planes (220), (311), (400), (422), (511) and (440) at 2θ values of 30.18°, 35.6°, 43.66°, 54.18°, 57.77° and 63.45°, respectively, consistent with the standard XRD data for the Fe_3O_4 phase (Fig. 1(a and b)). The average crystalline size of Fe_3O_4, OA-Fe_3O_4 nanorods were estimated using Debye–Scherrer formula, and the value obtained was about 25 ± 1and 32 ± 1, respectively. No additional peaks have been observed indicating the formation of pure and single phase without any impurities that remain from the un-reacted precursors. Moreover, it has been noticed that the peaks are broad and sharp that is an indication of the formation of very fine particles in the nanoscale range. The calculated inter d-spacing of crystalline structure determined for the reflected peak (311) from Bragg's law is 0.132 nm.

Fig. 2 depicts transmission electron microscopy (TEM) images of OA-Fe_3O_4 magnetite products. The well-suspended OA-Fe_3O_4 has been prepared in water and is drop cast onto a carbon coated copper grid for the TEM micrograph. Image (a) shows the TEM of OA-Fe_3O_4 magnetite nanorods which reveal that good dispersity of OA-Fe_3O_4 nanorods with sizes of about 30 ± 1 nm and results are accordance with XRD measurement. The coating of these nanorods is clearly visible in both images. The corresponding atomic scale image of the OA-Fe_3O_4 exhibits the well-organized lattice planes of Fe_3O_4 (image b).

3.2. Scanning electron microscope (SEM)

Fig. 3 shows the he surface morphology of (a) OA-Fe_3O_4/ITO electrodes and (b) BSA/Ab/OA-Fe_3O_4/ITO immunoelectrode has been confirmed by SEM images. Image (a) shows rod shape morphology which is uniform deposition of OA-Fe_3O_4 onto the ITO surface. After the immobilization of Ab and BSA onto OA-Fe_3O_4 electrode surface, the morphology of electrode has been changed and formed the globular shape morphology due to presence of macromolecular size of antibodies and BSA that confirm the presence of biomolecules (Ab, BSA) onto OA-Fe_3O_4/ITO electrode surface (image b).

3.3. Dynamic light scattering (DLS) study

The bare magnetite and OA capped NPs have been characterized using dynamic light scattering (DLS). It has been found that the hydrodynamic radius (R_H) of OA-Fe_3O_4 as 115.9 nm and Fe_3O_4 as 77.4 nm (data not shown). These results indicate that bare Fe_3O_4 is less hydrophilic as compared to OA capped Fe_3O_4 nanorods results indicated that Fe_3O_4 has been modified with OA. Table 1 shows particle size of bare Fe_3O_4 NPs and OA-Fe_3O_4 nanorods obtained from different techniques.

3.4. Fourier transforms infrared spectroscopy (FTIR) Study

Surface modification of OA/Fe_3O_4/ITO immunoelectrode after immobilization of Ab and BSA was confirmed by changing in IR spectra (Fig. 4). OA/Fe_3O_4/ITO, Ab/OA/Fe_3O_4/ITO and BSA/Ab/OA/Fe_3O_4/ITO immunoelectrode have been characterized by using FTIR. The IR spectrum shows main absorptions peak at 3400, 1500, 1090 and 591 cm^{-1}. The sharp peak in the spectrum around 591 cm^{-1} was ascribed to vibrations of Fe–O an iron oxide skeleton in almost all the samples (curve a), while the other absorptions should be assigned to organic species. The broad band around 3400 cm^{-1} was assigned to stretching vibrations of N–H bonds and adsorbed water molecules, the bands between 1385 and 1610 cm^{-1}were assigned to bending vibrations of N–H (amide I) and C–H bonds, and the peak at about 1090 cm^{-1} arises from the stretching vibrations of C–N bonds [33,34]. Compared with the uncoated magnetite nanorods, the larger intensity of the OH band (3400–3500 cm^{-1}) suggested that there was a reaction of the carboxylic acid group of acids with the surface hydroxyls of Fe_3O_4

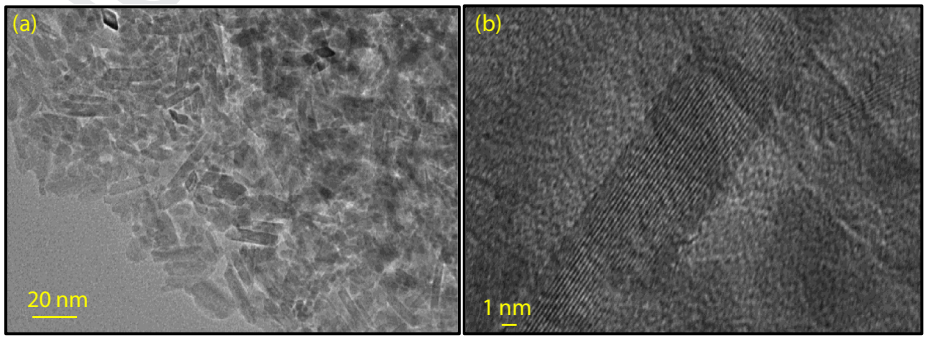

Fig. 2. (a) TEM images and (b) HRTEM of OA-Fe_3O_4 nanorods.

Please cite this article in press as: A. Sharma et al., Oxalic acid capped iron oxide nanorods as a sensing platform, Chemico-Biological Interactions (2015), http://dx.doi.org/10.1016/j.cbi.2015.05.020

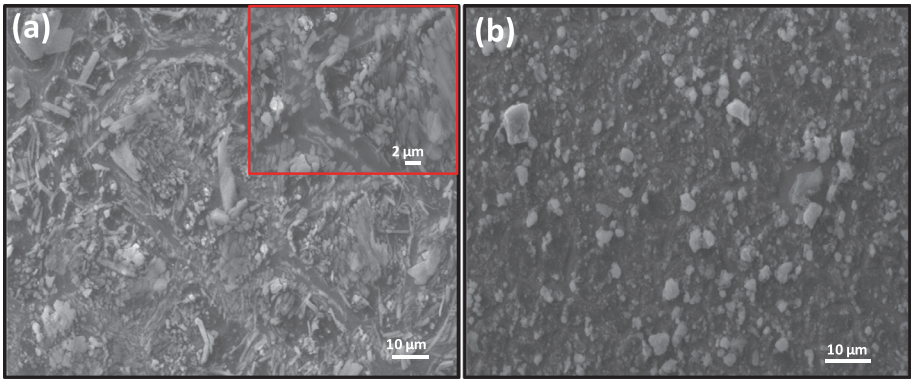

Fig. 3. SEM images shows (a) OA-Fe_3O_4/ITO electrode and (b) BSA/Ab/OA-Fe_3O_4/ITO immunoelectrode.

Table 1
Particle size of nanorods obtained from different techniques.

Nanorods	Nanorods size from XRD (nm)	Average nanorods size from TEM (nm)	Hydrodynamic radius from DLS (nm)
Fe_3O_4	29	24	77 (less hydrophobic)
OA caped Fe_3O_4	39	24	116

nanorods. The signature IR peaks appear at 1036 cm^{-1}, 1374 cm^{-1} (amide II) are responsible for carboxylate (COO^-) stretching (curve b). The broad hump formed in the region of 2994–3590 $cm^{-1}$is assigned to O–H stretching of carboxylic acid group. The presence of these peaks is evidence of the formation of oxalic acid capped Fe_3O_4 nanorods. However, the Fe–O vibration band at 500 cm^{-1} becomes broader and shifts towards higher wavenumber at 994 cm^{-1} may be due to the incorporation of BSA (curve d). The peaks seen at 1650 cm^{-1} and 1535 cm^{-1} indicating the presence of an amide band (I, II) and intensity increased at around 1250 cm^{-1} assigned to amide (III) revealing the immobilization of BSA onto the Ab/OA-Fe_3O_4/ITO electrode.

3.5. Zeta potential study

An imaginary surface (plane of shear) is used to represent the effective location of the solid–liquid interface, where the liquid velocity is zero. The equilibrium electric potential at the shear plane is called the zeta potential. The isoelectric point refers to the pH value at which zeta potential is zero. The surface charge potential of Fe_3O_4 in water could be explained by surface hydroxyl groups (Fe–OH). The presence of the hydroxyl group on the synthesized Fe_3O_4 nanorods surfaces was confirmed by infrared measurement as described. The zeta potential measurement gives the positive surface charge value of the bare Fe_3O_4 and OA-Fe_3O_4 nanorods. The value of zeta potential was found as 12.2, 8.4 mV for Fe_3O_4 and OA-Fe_3O_4, respectively (data not shown). The positive surface charge is expected due to the formation of Fe–OH_2^+ in an acidic environment. When OA was introduced into magnetite colloid solution, acid molecules preferred to attach to the surface of the nanorods because carboxylic acids of OA have a high affinity for metallic oxides. In this system, the Fe–OH bond at the surface of Fe_3O_4 reacted with the carboxylic acid group of the acid molecule *via* an acid–base reaction, giving Fe–O–C species with the elimination of H_2O [12].

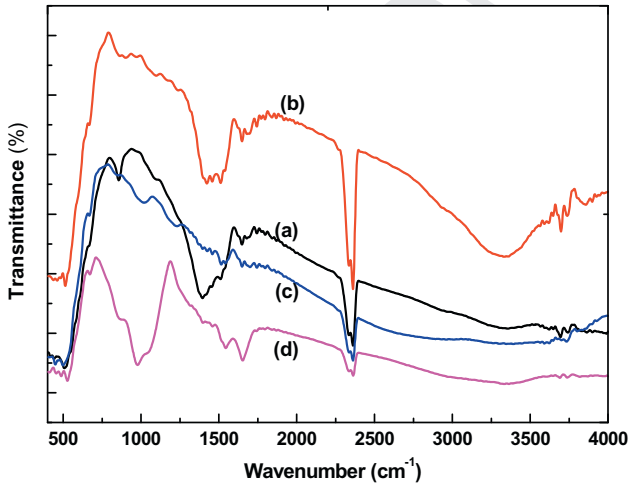

Fig. 4. FTIR spectra of (a) Fe_3O_4; (b) OA-Fe_3O_4/ITO electrode; (c) Ab/OA-Fe_3O_4/ITO; (d) BSA/Ab/OA-Fe_3O_4/ITO immunoelectrode.

3.6. Electrochemical studies

Cyclic voltammetric (CV) has been used to investigate the electrochemical behavior of Fe_3O_4/ITO and OA-Fe_3O_4/ITO electrodes prepared at different voltages (30–50 V) in phosphate buffer (50 mM, pH 6.0, 0.9% KCl) containing 3.3 mM $[Fe(CN)]_6^{3-/4-}$at scan rate of 20 mV/s (Fig. 5). We have optimized the film fabrication at different voltage and observed that the maximum oxidation and reduction magnitude of current of the electrolyte in three-electrode system at different voltage varies from 30 to 50 V and found that maximum current obtained at 30 V as shown in inset (Fig. 5). It may be due to deposition of small size nanorods attracted faster and deposited uniform thin film that enhanced fast electron transfer from electrolyte to electrode surface. While at higher voltage (40–50 V) large size nanorods deposited onto ITO surface to formed thick film and less uniformity resulting in slow charge transfer. So, all the electrodes have been fabricated at 30 V for further electrochemical studies.

The electrochemical response of (a) Fe_3O_4/ITO; (b) OA-Fe_3O_4/ITO; (c) Ab/OA-Fe_3O_4/ITO; (d) BSA/Ab/OA-Fe_3O_4/ITO immunoelectrode have been observed in phosphate buffer saline (50 mM, pH 6.0, 0.9% KCl) containing $[Fe(CN)_6]^{3-/4-}$ at scan rate of 20 mV/s (Fig. 5). It has been observed that the magnitude of oxidation current enhanced of OA-Fe_3O_4/ITO electrode (curve b) as compared to bare Fe_3O_4/ITO (curve a) as shown in Fig. 5. It may be due to OA capped Fe_3O_4 nanorods containing negative charge due to availability of carboxyl group facilitate fast transfer of electron originate from the negatively charged $[Fe(CN)_6]^{3-/4-}$ medium leading to enhanced heterogeneous electron transfer. Moreover, the enhancement of electrochemical signal due to self oxidation

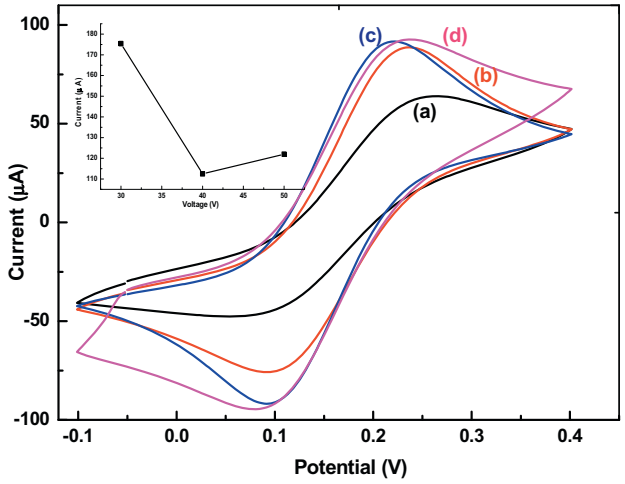

Fig. 5. CV of (a) Fe_3O_4/ITO; (b) OA-Fe_3O_4/ITO; (c) Ab/OA-Fe_3O_4/ITO; (d) BSA/Ab/OA-Fe_3O_4/ITO at scan rate of 20 mV/s and inset shows the current of OA-Fe_3O_4/ITO electrode as a function of deposition voltage.

of OA to carbon dioxide as mentioned in Eq. (4) [35]. However, the magnitude of current is increased and slightly shifted towards lower potential after the immobilization of antibodies onto OA-Fe_3O_4/ITO electrode resulting in reduced tunneling distance for diffusion of electrons from the bulk solution leading to enhanced current. It is due to the availability of gibbosities on OA-Fe_3O_4/ITO electrode surface facilitates the shorten distance and enhanced the magnitude of current due to improved heterogeneous electron transfer. These results indicate the significant increase in the heterogeneous electron transfer rate results due to strong interaction of antibodies with OA-Fe_3O_4/ITO electrode. However, the magnitude of current is not much changed but slightly shifted towards higher potential after incorporation of BSA onto Ab/OA-Fe_3O_4/ITO electrode (curve d).

$$HCOO{-}COOH \rightarrow 2CO_2 + 2H^+ + 2e^- \quad (4)$$

Fig. 6(A and B) shows the CV of OA-Fe_3O_4/ITO (A) and BSA/Ab/OA-Fe_3O_4 (B) immunosensor as a function of scan rate varying from 10 to 100 mV/s. It was observed that in both bioelectrodes the magnitude of both anodic (I_{pa}) and cathodic (I_{pc}) peak currents increased linearly with square root of the scan rate ($v^{1/2}$), suggesting that electrochemical reaction was a diffusion-controlled process.

The anodic (E_{pa}) and cathodic (E_{pc}) peak potentials and potential peak shifts ($\Delta E_p = E_{pa} - E_{pc}$) of OA-$Fe_3O_4$/ITO (A) and BSA/Ab/OA-$Fe_3O_4$/ITO immunoelectrode was observed to exhibit a linear relationship (linear regression coefficient 0.98) with the scan rate indicating facile charge transfer kinetics in the scan rate range from 10 to 100 mV s^{-1} in PBS containing 3.3 mM $[Fe(CN)_6]^{3-/4-}$. These results revealed that immunoelectrode provide sufficient accessibility to electrons between the electrolyte and the electrode. The diffusion co-efficient value of the redox species from the electrolyte to OA-Fe_3O_4/ITO and BSA/Ab/OA-Fe_3O_4/ITO immunoelectrode were calculated using the Randles–Sevcik [36] Eq. (5) as shown below. The obtained values have been mentioned in Table 1.

$$I_p = (2.69 \times 10^5) n^{3/2} A\, D^{1/2} C v^{1/2} \quad (5)$$

where I_p is the peak current of the BSA/Ab/OA-Fe_3O_4 immunoelectrode (I_{pa} anodic and I_{pc} cathodic), n is the number of electrons involved or electron stoichiometry, A is the surface area of the electrode (0.25 cm^2), D is the diffusion co-efficient, C is the concentration of redox species {3.3 mM $[Fe(CN)_6]^{3/4}$} and v is the scan rate (20 mV s^{-1}).

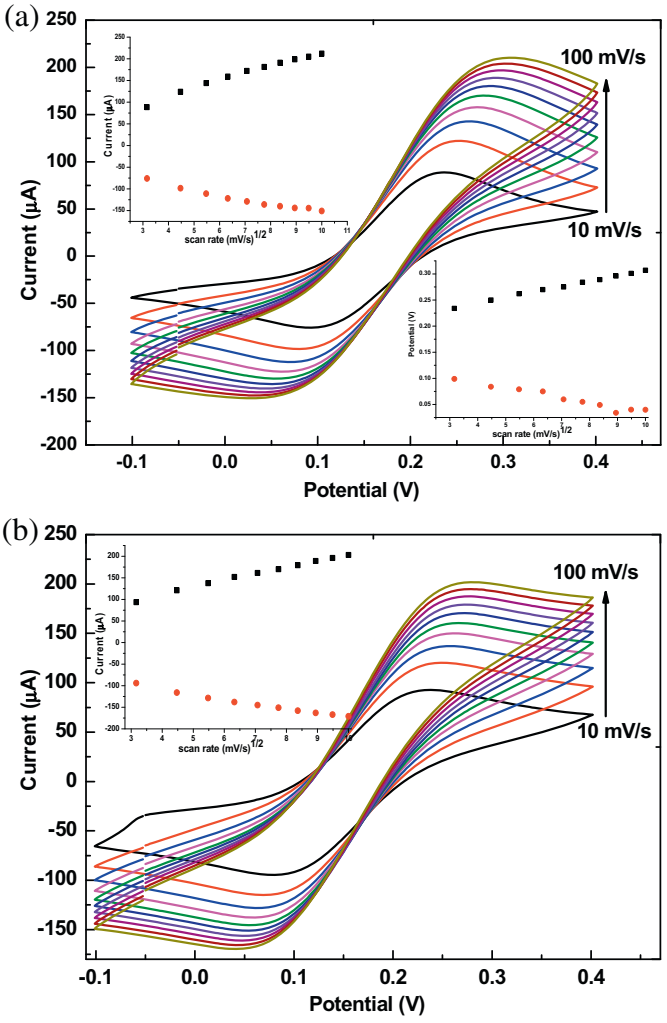

Fig. 6A and B. Shows CV of OA-Fe_3O_4/ITO and BSA/Ab/OA-Fe_3O_4/ITO immunoelectrode as a function of scan rate from 10 to 100 mV/s. Inset shows the graph of current with $\sqrt{\text{scan rate}}$.

The electroactive surface area (A_e) of the OA-Fe_3O_4/ITO and BSA/Ab/OA-Fe_3O_4/ITO immunoelectrode was determined from the calculated diffusion co-efficient and the Randles–Sevcik equation [36].

$$A_e = S/(2.99 \times 10^5) n^{3/2} C D^{1/2} \quad (6)$$

where S is the slope of the straight line obtained from the graph of I_p versus scan $rate^{1/2}$. The A_e value of the OA-Fe_3O_4/ITO (A) and BSA/Ab/OA-Fe_3O_4/ITO immunoelectrode has been found to be 0.62 and 0.53 mm^2, respectively.

The surface concentration of ionic species of these electrodes was estimated using Brown–Anson model [36].

$$I_p = \frac{n^2 F^2 \Gamma^* A V}{4RT} \quad (7)$$

where n is the number of electrons transferred which is 1 in this case, F is Faraday constant (96485.34 C mol^{-1}), A is surface area of the electrode (0.25 cm^2), R is gas constant, Γ^* is surface concentration of ionic species of immunoelectrodes (mol/cm^2), T is 298 K, and I_p/V is the slope of calibration plot (scan rate value). The surface concentration of OA-Fe_3O_4/ITO and BSA/Ab/OA-Fe_3O_4/ITO immunoelectrode was found to be 1.9×10^{-8} and 1.99×10^{-8} M/cm^2,

respectively. The results indicate that OA-Fe_3O_4/ITO electrode provides increased electroactive surface area for loading of antibodies (Ab). However, after the immobilization of Ab, the surface concentration changed confirms the presence of Ab and BSA ontoOA-Fe_3O_4/ITO electrodes surface with multilayer coverage.

The value of the heterogeneous electron transfer rate constant (K_s) obtained for OA-Fe_3O_4/ITO and BSA/Ab/OA-Fe_3O_4/ITO immunoelectrode was estimated to be 0.11 and 0.12 s^{-1} according to the model of Laviron as in eq. (8) [37].

$$K_s = mnFv/RT \quad (8)$$

where m is the peak-to-peak separation (0.14 and 0.15 V, respectively), The highest value of K_s was found in case of OA-Fe_3O_4/ITO electrode as compared to BSA/Ab/OA-Fe_3O_4/ITO immunoelectrode, Table 2 shows the electrochemical parameters: anodic peak current (I_{pa}), cathodic peak current (I_{pc}), charge transfer rate constant (K_s), diffusion coefficient (D), electroactive surface area (A_e), average surface concentration (I^*) of ionic species obtained for respective electrodes.

3.7. Electrochemical impedance spectroscopy study

Electrochemical impedance spectroscopy (EIS) is an effective tool for studying interfacial properties of surface modified electrodes. In the EIS, the semicircular diameter of the EIS spectra gives a value of the charge transfer resistance (R_{CT}) that reveals electron transfer kinetics of the redox probe at the electrode interface. Moreover, R_{CT} depends on dielectric characteristics of the electrode/electrolyte interface. The EIS studies has been investigated in PBS containing 3.3 mM $[Fe(CN)_6]^{3-/4-}$ in the frequency range 0.01 –10^5 Hz. The semicircular part corresponds to the electron transfer limited process; its diameter is equal to the electron transfer resistance (R_{CT}) which controls the electron transfer behavior of the redox probe at the electrode interface. Fig. 6(C) shows the Nyquist plot of the impedance of respective modified electrodes (a) Fe_3O_4/ITO; (b) OA-Fe_3O_4/ITO; (c) Ab/OA-Fe_3O_4/ITO and (d) BSA/Ab/OA-Fe_3O_4/ITO immunoelectrodes. It has been observed that R_{CT} for Fe_3O_4/ITO electrode (curve a) is smaller than that of OA/Fe_3O_4/ITO electrode (curve b). This suggests that Fe_3O_4/ITO electrode improved conductivity of the electrode and that the positively charged which facilitate diffusion of the negatively charged $[Fe(CN)_6]^{3-/4-}$ ions towards the electrode surface. After the immobilization of Ab onto the OA-Fe_3O_4/ITO electrode, the R_{CT} value decreases, revealing that non-binding sites on Ab facilitate electron transfer between the OA-Fe_3O_4/ITO electrode and electrolyte. Further, R_{CT} decreases after the immobilization of BSA onto the Ab/OA-Fe_3O_4/ITO, revealing that BSA blocks non-specific sites onto Ab/OA-Fe_3O_4/ITO that perhaps perturb electron communication between the BSA/Ab/OA-Fe_3O_4/ITO immunoelectrode and ITO surface.

3.8. Electrochemical response studies

The EIS response studies of the BSA/Ab/OA-Fe_3O_4/ITO immunoelectrode were conducted as a function of *V. cholerae* concentration

Table 2
Shows the electrochemical parameters: anodic peak current (I_{pa}), cathodic peak current (I_{pc}), charge transfer rate constant (K_s), diffusion coefficient (D), electroactive surface area (A_e), average surface concentration (I^*) for respective electrodes.

Electrodes	I_{pa} (μA)	I_{pc} (μA)	K_s (s^{-1})	D ($cm^2\ s^{-1}$)	A_e (mm^2)	I^* (mol cm^{-2})
Fe_3O_4/ITO	65.4	−46.2	0.14	4.34×10^{-12}	–	1.39×10^{-8}
OA-Fe_3O_4/ITO	89.6	−76.7	0.11	8.15×10^{-12}	0.62	1.9×10^{-8}
BSA/Ab/OA-Fe_3O_4/ITO	93.7	−94.96	0.12	8.9×10^{-12}	0.53	1.99×10^{-8}

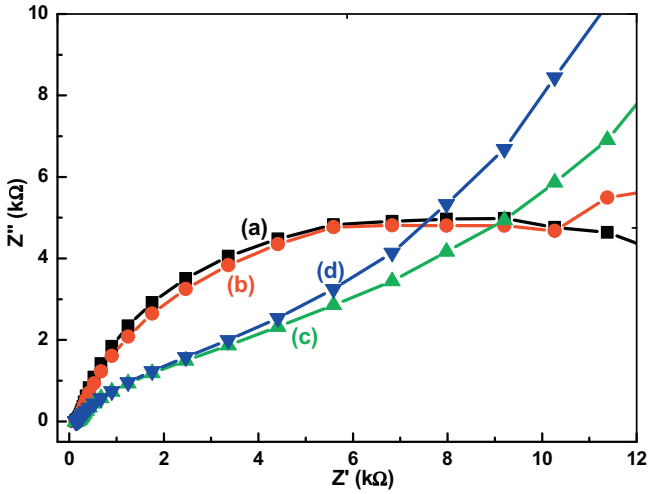

Fig. 6C. Shows Nyquist plot of (a) Fe_3O_4/ITO; (b) OA-Fe_3O_4/ITO; (c) Ab/OA-Fe_3O_4/ITO and (d) BSA/Ab/OA-Fe_3O_4/ITO immunoelectrode at zero potential in PBS containing 3.3 mM $[Fe(CN)_6]^{3-/4-}$.

(12.5–400 ng/mL) in PBS containing $[Fe(CN)_6]^{3-/4-}$ containing 3.3 mM $[Fe(CN)_6]^{3-/4-}$as shown in Fig. 7. The BSA/Ab/OA-Fe_3O_4/ITO immunoelectrode were treated with 30 mL of *V. cholerae* concentration and then incubated for ten minutes at room temperature (25 °C). It was found that the R_{CT} value decreases with increasing concentrations of antigen (*Vibrio cholera*). It may be due to antibody-antigen complex formation which enhanced the charge transfer rate resulting in decrease R_{CT} value and increased sensitivity (inset Fig. 7). The detection range found as 12.5–500 $ngmL^{-1}$ with low detection limit of 0.5 ng mL^{-1}calculated by using the $3\sigma_b/m$ criteria, where m is slope of the calibration graph and σ_b is the standard deviation of the blank signal. The sensitivity of the BSA/Ab/OA-Fe_3O_4/ITO calculated by the slope of the linear regression curve is 0.1 Ω/ng $mL^{-1}cm^{-2}$, which is higher than the previous reported CA-Fe_3O_4 nanoparticles. The electrochemical response studies of bare Fe_3O_4 (uncapped) based BSA/Ab/Fe_3O_4/ITO immunoelectrode have been conducted as a function of *V. cholerae* concentration at similar condition [Data not shown]. It has been

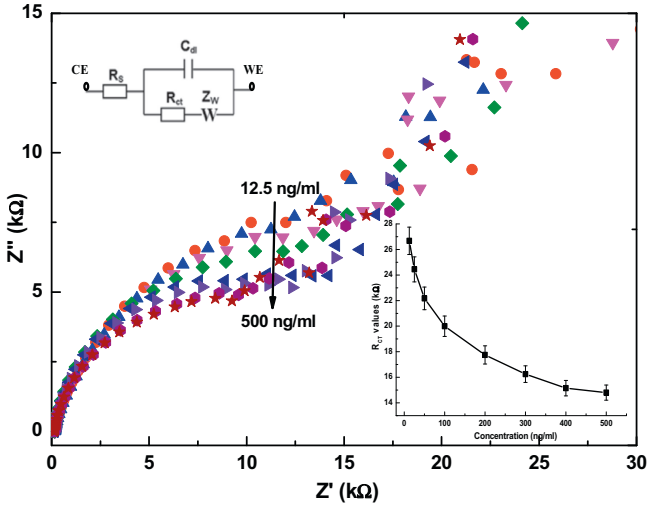

Fig. 7. Shows electrochemical response studies of BSA/Ab/OA-Fe_3O_4/ITO as a function of antigen concentration of 12.5–400 ng/ml and inset shows the respective R_{CT} values at zero potential in PBS containing 5 mM $[Fe(CN)_6]^{3-/4-}$ (inset (A): Randles equivalent circuit, where R_s: solution resistance, R_{CT}: charge transfer resistance, Z_w: Warburg impedance, and C_{dl}: double layer capacitance).

Table 3
Shows a comparative biosensing characteristics of BSA/Ab/OA-Fe_3O_4/ITO immunoelectrode along with reported in literature.

Electrode/ immobilization/transducer	Transducer	Biomolecules	Detection range	Low detection range	Sensitivity	Refs.
BSA/Ab/CA-Fe_3O_4/ITO	Electrochemical impedance spectroscopy	Antibodies	12.5–500 ng ml^{-1}	0.32 ng ml^{-1}	0.03 Ω/ng $ml^{-1}cm^{-2}$	[19]
Nickel oxide nanowires/ITO	Electrochemical impedance spectroscopy	Antibodies	37–350 ng ml^{-1}	0.553 ng ml^{-1}	11.12 Ω/ng $ml^{-1}cm^{-2}$	[25]
RGO-TiO_2/ITO	Electrochemical impedance spectroscopy	Antibodies	10–450 ng/mL	0.15 ng mL^{-1}	21.8 × 10^{-3} μF/ ng mL^{-1}/cm^2	[26]
Lipid layer	Chemiluminescence	HRP/ganglioside GM1	1 pgmL^{-1}–1 ngmL^{-1}	0.8 pgmL^{-1}	–	[27]
Gold-coated AFM microcantilevers	Dynamic force microscopy	Antibodies	1 × 10^3–1 × 10^7 CFU/ml.	1 × 10^3 CFU/ml,	~146.5 pg/Hz	[28]
BSA/Ab/OA-Fe_3O_4/ITO	Electrochemical impedance spectroscopy	Antibodies	12.5–500 ng ml^{-1}	0.5 ng ml^{-1}	0.1 Ω/ng $ml^{-1}cm^{-2}$	Present work

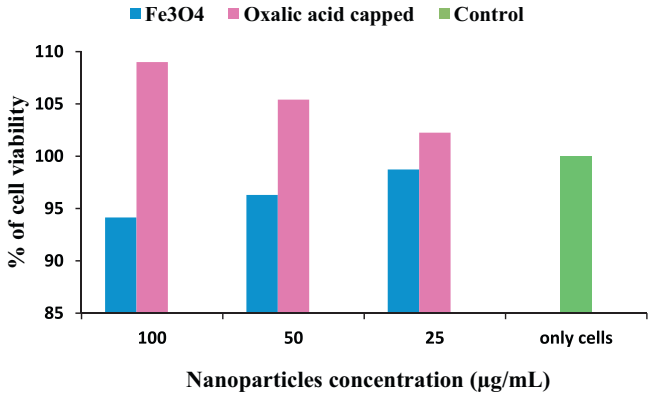

Fig. 8. Effect of Fe_3O_4 and OA-Fe_3O_4 Nanorods on the proliferation of HEK 293 cells.

observed that the R_{CT} value does not change significantly as compared to OA capped Fe_3O_4 nanorods based [BSA/Ab/OA-Fe_3O_4/ITO] immunoelectrode. These results indicate that the OA-Fe_3O_4 nanorods [BSA/Ab/OA-Fe_3O_4/ITO] immunoelectrode shows higher interaction of antibodies with antigens and exhibits improved biosensing properties. The stability of BSA/Ab/OA-Fe_3O_4/ITO immunoelectrode obtained 50 days (80%) and reproducibility more than 11 times. Table 3 shows the comparison of biosensing properties of BSA/Ab/OA-Fe_3O_4/ITO immunoelectrode along with reported in literature.

3.9. Effect of cytotoxicity

Fig. 8 shows the relative percentage proliferation of HEK 293 cells in the presence of Fe_3O_4 and OA-Fe_3O_4 nanorods, respectively; in the concentration range 0–100 μg mL^{-1}. The MTT assay results indicated that viability of HEK 293 is not affected in the presence of Fe_3O_4 and OA-Fe_3O_4 nanorods, resulted normal growth of cells. These results suggest that nanorods are biocompatible and do not have toxic affect on human cells *in vivo* studies. However, the OA-Fe_3O_4 nanorods exhibit higher biocompatibility over Fe_3O_4 indicated that OA-Fe_3O_4 nanorods facilitate cell growth. Similar results reported with Hela cell lines [38].

4. Conclusions

Biocompatible magnetite nanorods prepared by co-precipitation method and stabilized by coating with oxalic acid (OA). We have successfully functionalized Fe_3O_4 nanorods with OA that confirmed by TEM, FTIR and DLS. These NPs has been deposited using electrophoretic deposition technique onto ITO surface for immobilization of monoclonal antibodies against *V. cholerae* and BSA for *V. cholerae* detection using impedimetric techniques. The results of these studies obtained as linearity 12.5–500 ng mL^{-1} with low detection limit of 0.5 ngmL^{-1}, sensitivity 0.1 Ω/ng $mL^{-1}cm^{-2}$ and reproducibility more than 11 times. This type of electrode has the potential to be of general use for designing new electrochemical immunosensors for detection of other clinically important antigens.

Transparency Document

The Transparency document associated with this article can be found in the online version.

Acknowledgements

AS and DB acknowledges University Grants Commission, Government of India for a research fellowship. This work was supported by a Grant received from Department of Science and Technology, Government of India (Grant no. SB/PC/S1/110/2012). Authors are thankful to the Advanced Instrument Research Facility of the University for providing access to FTIR and SEM instruments.

References

[1] P.R. Solanki, A. Kaushik, V.V. Agrawal, B.D. Malhotra, Nanostructured metal oxide-based biosensors, NPG Asia Mater. 3 (1) (2011) 17–24.
[2] R. Sharma, V.V. Agrawal, A.K. Srivastava, Govind, L. Nain, M. Imran, S.R. Kabi, R.K. Sinha, B.D. Malhotra, Phase control of nanostructured iron oxide for application to biosensor, J. Mater. Chem. B 1 (2013) 464–474.
[3] E. Amstad, M. Textor, E. Reimhult, Stabilization and functionalization of iron oxide nanoparticles for biomedical applications, Nanoscale 3 (2011) 2819–2843.
[4] Y.F. Rao, W. Chen, X.G. Liang, Y.Z. Huang, J. Miao, L. Liu, Y. Lou, X.G. Zhang, B. Wang, R.K. Tang, Z. Chen, X.Y. Lu, Epirubicin-loaded superparamagnetic iron-oxide nanoparticles for transdermal delivery: cancer therapy by circumventing the skin barrier, Small 11 (2) (2015) 239–247.
[5] G.K. Kouassi, J. Irudayaraj, G. McCarty, Examination of cholesterol oxidase attachment to magnetic nanoparticles, J. Nanobiotechnol. 3 (1) (2005) 1–9.
[6] T.R. Pisanic, J.D. Blackwell, V.I. Shubayev, R.R. Finones, S. Jin, Nanotoxicity of iron oxide nanoparticle internalization in growing neurons, Biomaterials 28 (16) (2007) 2572–2581.
[7] Y. Wang, J. Dostalek, W. Knoll, Magnetic nanoparticle-enhanced biosensor based on grating-coupled surface plasmon resonance, Anal. Chem. 83 (16) (2011) 6202–6207.
[8] A. Kaushik, R. Khan, P.R. Solanki, P. Pandey, J. Alam, S. Ahmad, B.D. Malhotra, Iron oxide nanoparticles–chitosan composite based glucose biosensor, Biosens. Bioelectron. 24 (2008) 676–683.
[9] A. Kaushik, P. R. Solanki, K. Kaneto, C. G. Kim, Sharif Ahmad, Bansi D. Malhotra, Nanostructured iron oxide platform for impedimetric cholesterol detection, Electroanalysis, 22 (10) (2010) 1045 – 1055.
[10] G. Zhao, J.J. Feng, Q.L. Zhang, S.P. Li, H.Y. Chen, Syntheisis and characterization of prussian blue modified magnetite nanoparticles and its application to the electrocatalytic reduction of H_2O_2, Chem. Mater. 17 (2005) 3154–3159.

[11] A.K. Gupta, R.R. Naregalkar, V.D. Vaidya, M. Gupta, Recent advances on surface engineering of magnetic iron oxide nanoparticles and their biomedical applications, Nanomedicine (2007) 223–239.
[12] S. Yu, G.M. Chowa, Carboxyl group (–CO_2H) functionalized ferrimagnetic iron oxide nanoparticles for potential bio-applications, J. Mater. Chem. 14 (2004) 2781–2786.
[13] S. Nigam, K. Barick, D. Bahadur, Development of citrate-stabilized Fe_3O_4 nanoparticles: conjugation and release of doxorubicin for therapeutic applications, J. Magn. Magn. Mater. 323 (2011) 237–243.
[14] C. Boyer, M.R. Whittaker, V. Bulmus, J. Liu, T.P. Davis, The design and utility of polymer-stabilized iron-oxide nanoparticles for nanomedicine applications, NPG Asia Materials 2 (2010) 23–30.
[15] E. Munnier, S. Cohen-Jonathan, C. Linassier, L. Douziech-Eyrolles, H. Marchais, M. Souce, K. Herve, P. Dubois, I. Chourpa, Novel method of doxorubicin–SPION reversible association for magnetic drug targeting, Int. J. Pharm. 363 (2008) 170–176.
[16] L. Li, K. Mak, C. Leung, K. Chan, W. Chan, W. Zhong, P. Pong, Synthesis and characterization of self-Assembled monolayer and bilayer carboxyl-group functionalized magnetic nanoparticles, IEEE Trans. Magn. 48 (2012) 3299–3302.
[17] M.A. Daniele, M.L. Shaughnessy, R. Roeder, A. Childress, Y.P. Bandera, S. Foulger, Magnetic nano clusters exhibiting protein-activated near-infrared fluorescence, ACS Nano 7 (2013) 203–213.
[18] C. Liu, P.M. Huang, Atomic force microscopy and surface characteristics of iron oxides formed in citrate solutions, Soil Sci. Soc. Am. J. 63 (1999) 65–72.
[19] A. Sharma, D. Baral, K. Rawat, P.R. Solanki, H.B. Bohidar, Biocompatible capped iron oxide nanoparticles for Vibrio cholerae detection, Nanotechnology 26 (2015) 175302 (10pp).
[20] M.E. De Sousa, M.B.F.V. Raap, P.C. Rivas, P.M. Zelis, P. Girardin, G.A. Pasquevich, J.L. Alessandrini, D. Muraca, F.H. Ssnchez, Stability and relaxation mechanisms of citric acid coated magnetite nanoparticles for magnetic hyperthermia, J. Phys. Chem. C 117 (10) (2013) 5436–5445.
[21] E. Cheraghipour, S. Javadpour, A.R. Mehdizadeh, Citrate capped superparamagnetic iron oxide nanoparticles used for hyperthermia therapy, J. Biomed. Sci. Eng. 5 (2012) 715–719.
[22] I. Palchetti, M. Mascini, Electroanalytical biosensors and their potential for food pathogen and toxin detection, Anal. Bioanal. Chem. 391 (2) (2008) 455–471.
[23] O. Lazcka, C.F.J. Del, M.F. Xavier, Pathogen detection: a perspective of traditional methods and biosensors, Biosens. Bioelectron. 22 (2007) 1205–1217.
[24] S. Viswanathan, W. Li-chen, M.R. Huang, H.J. Annie, Electrochemical immunosensor for cholera toxin using liposomes and poly(3,4-ethylenedioxythiophene)-coated carbon nanotubes, Anal. Chem. 78 (4) (2006) 1115–1121.
[25] P.R. Solanki, M.A. Ali, V.V. Agrawal, A.K. Srivastava, R.K. Kotnala, B.D. Malhotra, Highly sensitive biofunctionalized nickel oxide nanowires for nanobiosensing applications, RSC Adv. 3 (2013) 16060–16067.
[26] P.R. Solanki, S. Srivastava, M.A. Ali, R.K. Srivastava, A. Srivastava, B. Malhotra, RSC Adv. 4 (104) (2014) 60386–60396.
[27] U. Sungkanak, A. Sappat, A. Wisitsoraat, C. Promptmas, A. Tuantranont, Biosens. Bioelectron. 26 (2) (2010) 784–789.
[28] H. Chen, Y. Zheng, J.H. Jiang, H.L. Wu, G.L. Shen, R.Q. Yu, Biosens. Bioelectron. 24 (4) (2008) 684–689.
[29] Y.S. Kang, S. Risbud, J.F. Rabolt, P. Stroeve, Synthesis and characterization of nanometer-size Fe_3O_4 and γ-Fe_2O_3particles, Chem. Mater. 8 (1996) 2209–2211.
[30] M. Racuciu, D.E. Creang, A. Airinei, Citric-acid-coated magnetite nanoparticles for biological applications, Eur. Phys. J. E 21 (2) (2006) 117–121.
[31] R. Shinar, J. Shinar: Organic electronics in sensors and biotechnology. Electrophoretically deposited polymers for organic electronics, chapter by C. Dhand and B.D. Malhotra (McGraw-Hill Professional, 2009), Access Engineering.
[32] B.J. Berne, R. Pecora, Dynamic light scattering with applications to chemistry biology and physics, Wiley-Interscience, New York, USA, 1976.
[33] H. Ohshima, Electrophoresis of soft particles, Adv. Colloid Interface Sci. 62 (1995) 189–235.
[34] Y. Tian, B. Yu, X. Li, K. Li, Facile solvothermal synthesis of monodisperse Fe_3O_4 nanocrystals with precise size control of one nanometre as potential MRI contrast agents, J. Mater. Chem. 21 (2011) 2476–2481.
[35] L.C. Rockombeny, J.P. Feraud, B. Queffelec, D. Ode, T. Tzedakis, Electrochemical oxidation of oxalic acid and hydrazinium nitrate on platinum in nitric acid media, Electrochim. Acta 66 (2012) 230–238.
[36] A.J. Bard, L.R. Faulkner, A digital simulation model for electrochromic processes at WO3 electrodes, John Wiley & Sons, New York, 1980.
[37] J. Singh, A. Roychoudhury, M. Srivastava, P.R. Solanki, D.W. Lee, S.H. Lee, B.D. Malhotra, A highly efficient rare earth metal oxide nanorods based platform for aflatoxin detection, J. Mater. Chem. B 1 (2013) 4493–4503.
[38] S. Nigam, K.C. Barick, D. Bahadur, Development of citrate-stabilized Fe_3O_4 nanoparticles: conjugation and release of doxorubicin for therapeutic applications, J. Magnetism Magnet. Mater. 323 (2011) 237–243.

Please cite this article in press as: A. Sharma et al., Oxalic acid capped iron oxide nanorods as a sensing platform, Chemico-Biological Interactions (2015), http://dx.doi.org/10.1016/j.cbi.2015.05.020